J. Earth & Space Physics. Vol. 29, No. 1 (2003) P. 1-12

Mountain drag and adjustment to equilibrium: A numerical study

Farahani, M. M. [*] and Wu, R. [**]

[*] *Institute of Geophysics, University of Tehran, P. O. Box 14155-6466, Tehran, Iran.*
[**] *Department of Atmospheric Sciences, Nanjing University, Nanjing 210093, China.*
Received: 23 Jul. 2002 *Accepted: 16 Sep. 2003*

Abstract

Series of experiments is carried out to investigate the influence of a mountain on air flows around and over it. Experiments were concentrated on the role of orography in the adjustment process. Based on the results of experiments, we find that: (I) the final equilibrium state of the atmosphere is not geostropically balanced. The height of mountain influences the adjustment period; higher mountains make the adjustment period longer. (II) Fronts are not observed during geostrophic adjustment, unlike what was suggested before. Although frontal features appear on the maps, their length scales are shorter than those of the atmospheric fronts. (III) The ratios of kinetic energy to the potential energy released during adjustment are smaller and larger than those predicted by the theory when, kinetic energy is computed from respectively geostrophic and actual winds. (IV) For small Froude numbers, the relation between mountain drag and Froude number is more complicated than what has already been suggested. (V) In the nonlinear regime studied here, splitting of flow and vertically propagating internal gravity waves are found as other major mechanisms for drag development in addition to the three possibilities suggested by Smith for linear regimes.

Key words: Adjustment, Front, Mountain Drag, Energetic of adjustment process

1. Introduction

The Earth's surface over continents is not flat, at least over distances of more than a few kilometers. Often, surface elevation varies over scales much smaller than this. The effects of orography have been studied by many meteorologists. Our current understanding of the effects of mountains on flows over them is mainly based on two-dimensional linear analyses and two-dimensional numerical simulations. Mountains play a significant role in modifying regimes of flow in neutral atmospheric boundary layers. They have a more pronounced effect in the adjustment process of an atmosphere with unbalanced wind and mass fields. The effects of surface features on airflow around and over them are important for a number of reasons. Changing local climate, acting as a sink of energy of the atmosphere, affecting meteorologically important parameters such as pressure, temperature and wind beneath it, modifying flow in the free atmosphere and acting as generating mechanism for atmospheric waves, especially gravity waves, are among the reasons that mountains have remained in the centre of attention of atmospheric scientists for a long time.

One of the above effects is the influence of mountain on airflow during the geostrophic adjustment process. During its evolution, the later process involves other meteorologically interesting and important features, the most remarkable of which is front and the process of frontogenesis. Ou (1984) considered the mechanism of frontogenesis during the process of geostrophic adjustment. Blumen and Wu (1995) and Wu and Blumen (1995), from now on WB, studied the frontogenesis by applying three conservation principles in two dimensions. Farahani and Wu (1998), from now on FW, made a numerical effort to investigate the problem with more realistic 3-dimensional model, data, and initial conditions. All of these works found that for specific conditions fronts occur. FW suggested that the main reason or mechanism of occurrence of fronts is the changes in streamlines and generation of a deformation field on the maps of airflow. In FW, numerical simulations started from idealized, dynamically unbalanced fields with a flat-surface lower boundary. More precisely, WB's initial conditions were used for mass and wind fields. FW raised the question of " how would the adjustment process change, if the surface level included the topography and non-flat obstacles? ". Answering this question is the main motivation for us to further investigate the influence of orography on adjustment.

Recently focus has been on two important aspects of mountains: gravity waves ('splitting flow' and breaking waves) and mountain Drag. The role of gravity waves has been recognized for a long time and was introduced initially by Eliassen and Palm (1961). This idea took a long time to be practically exploited in routine weather

forecasting models, by Palmer et al. (1986) and McFarlane (1987) in parameterization schemes. Drag effect, as a sink of energy resulting from surface raggedness is another important parameter that should be taken into account. This parameter took attention of theoreticians and was first studied in linear case by Smith (1978), who found that the splitting of the flow around the mountains happens for a sufficiently small Froude number. He also found that the drag occurs when the unperturbed wind has a component perpendicular to the ridge. According to Smith (1978), the splitting of flow is not sufficient for wave drag, but requires blocking of the surface flow upstream.

Miranda and James (1992) carried out some numerical experiments to investigate the effects of mountains on the gravity waves. They applied a 3-dimensional, non-hydrostatic model to see the Froude-number dependency of the flow passing a 3-dimensional mountain. Their model employed nonlinear equations and the frictionless stratified flow. The main drawback was using a constant value (zero) for f (Coriolis parameter). Although for their purpose and the domain they used (80 km) such a simplification is reasonable, for simulating the real atmosphere for larger domains and wider mountains it is not. In the present study, our objective is to examine the role of mountains in adjustment process and to verify the analytically predicted phenomena similar to those of Smith, as well as the magnitude of mountain drag in different conditions. Since Ou, WB and FW have found a specific relation between released potential energy and created kinetic energy within the adjustment process, and since drag behaves as a sink of energy, in our study we anticipate some differences in energetic of the problem with previous results.

Here we apply the Pennsylvania State University (PSU) and National Center for Atmospheric Research (NCAR) Meso-scale Model version 4 (MM4) as our research model and run it for different types of initial conditions and different heights and widths of mountains. In section 2, a brief introduction to the model and its set-up for our tests is given. Section 3 discusses the meteorological data used for initial state and the shapes of the mountains in our simulations. Section 4 is devoted to the results of the experiments and our major achievements. The behaviors of energy and mountain drag in our experiments are discussed in sections 5 and 6, respectively. The conclusions and remarks are given in section 7.

2. Description of the MM4

The model was introduced by Anthes and Warner (1978) at the PSU and NCAR in 1978. Since then, different versions of the model have been developed, introduced and used as routine meso-scale forecasting model in many operational centers. Present study employs version eight of the fourth generation of MM4. The complete descriptions of the model along with the full set of equations can be found in Anthes and Warner (1978) and Hsie (1987). A brief description of MM4 is given here. The model is hydrostatic. The boundary layer treatment is according to Blackadar's (1976) parameterization. In horizontal surfaces of model's domain, the prognostic variables are defined according to Arakawa B-grid (Haltiner and Williams 1980). Therefore horizontal grid structure is staggered with the x and y components of momentum defined at odd grid points and all other variables at even grid points. In vertical direction, the model uses terrain-following staggered σ (scaled pressure, P) coordinate, with vertical velocity $\dot{\sigma}$ at full levels and all other variables at half levels. This choice of vertical coordinate has some practical advantages resulting from a simplification of the thermodynamic calculations, and the fact that observational data are on constant pressure levels. However, there is a main disadvantage for this vertical-coordinate system, that is, the equations admit a fast external, acoustic mode (Lamb mode). A time-splitting technique is used to handle fast modes and to eliminate them efficiently. Shorter time scales could slow down or remove these fast moving waves and reduce their effects on predicted variables. Initialization process of the model includes, normal-mode initialization technique, in lateral boundaries boundary nudging method, Four Dimensional Data Assimilation (FDDA), and diabatic and adiabatic processes. The numerical solution technique used is the finite difference that approximately conserves mass, momentum, and total energy. This solving technique is consistent with the WB's assumptions and thus it is expected to be able to give a satisfactory representation of the net influence of mountain on the drag coefficient. The boundary condition in the lowest level of model's domain is $D\sigma/Dt=0$. The details of initial and lateral boundary conditions will be given in the next section.

3. Set-up of the experiments

The set-up processes of the experiments consist of two parts: (I) preparation of the initial data, and (II) set-up of the model's parameters for different experiments.

(I) *Preparation of the initial data.* A standard version with 10 σ layers of MM4 is used as our numerical model. The selected σ levels are 1.0, 0.9, 0.8, 0.7, 0.6,

Table 1. :parameters and results of experiments For the names of the experiments and acronyms used in this table see the text.

Expt.	h_0	*a*	*b*	*Dx*	*BY*	*D2*	*T*	*N*	*U*	*F*	γ_R	γ_G	$Drag/D_{hydrostatic}$	$Drag/D_{nonhydrostatic}$	Comment
C1T1	500	10	10	10	10	15	10	1.37	14.35	2.1	4.3	0.76	4.36	3.30	
C1T2	1000	10	10	10	10	15	11	1.37	15.1	1.1	4.8	1.99	2.66	2.04	
C1T3	2000	10	10	10	10	15	15	1.37	12.8	0.47	4.6	8.1	1.67	1.23	
C1T4	3000	10	10	10	10	15	18	1.37	10.61	0.26	4.5	17.9	1.96	1.35	
C1T5	1000	10	10	5	10	15	9	1.43	7.25	0.51	1.6	20.2	13.05	7.58	
C1T6	2000	10	10	5	10	15	14	1.44	4.6	0.16	1.6	85.4	14.29	5.69	
C1T7	1000	20	20	10	10	15	17	1.38	11.0	0.8	4.5	5.30	2.52	1.26	
C1T8	1000	30	30	10	10	15	24UP	1.4	5.46	0.39	4.3	7.6	4.91	0.74	still not stable
C2T1	1000	10	10	10	4	8	11	1.4	12.47	0.89	2.3	1.96	1.76	1.28	
C2T2	2000	10	10	10	4	8	13	1.4	12.19	0.43	2.2	7.6	1.7	1.23	
C2T3	3000	10	10	10	4	8	22	1.48	8.52	0.19	3.0	103.3	7.43	4.7	Front after 7 hr.
					A	***B***									
C3T1	500	10	10	10	-10	40	14	1.54	2.85	0.37	3.1	0.7	3.41	0.96	
C3T2	0	0	0	10	-10	40	10	1.5	3.81	∞	3.0	0.57	—	—	
C3T3	500	10	10	10	-20	50	17	1.52	3.0	4.01	7.1	2.56	3.21	0.97	
C3T4	0	0	0	10	-20	50	12.5	1.5	3.65	∞	7.1	2.4	—	—	
C3T5	1000	20	20	10	-15	50	18	1.57	3.43	0.22	5.6	3.6	5.5	.75	
C3T6	2000	20	20	10	-15	50	20	1.58	3.92	0.12	5.8	10.2	3.5	0.6	
C3T7	3000	20	20	10	-15	50	22	1.59	4.6	0.096	6.0	21.3	2.6	0.56	

0.5, 0.4, 0.3, 0.2, 0.1, 0.0, corresponding to pressure levels 1000, 910, 820, 730, 640, 550, 460, 370, 280, 190, 100 hPa, respectively. On every σ level, our horizontal grid consists of 31×31 equally-spaced points.

In all experiments reported here, the date used for both initial-state meteorological variables and topography, are idealized. For topography, we follow previous theoretical works on this topic such as Smith (1980) and Miranda and James (1992), and use circular bell-shaped mountains with different heights and widths. The height of mountain is computed according to the following relation;

$$h = h_0\left\{1+\left(\frac{x-x_0}{a}\right)^2+\left(\frac{y-y_0}{b}\right)^2\right\}^{-3/2} \qquad (1)$$

where h_0 is the maximum height, a and b are half-widths of the mountain in kilometer in x and y direction and x_0 , y_0 are the coordinates of the top of the bell-shaped mountain which is centered in our model domain. Also note that the two parameters a and b control the slope of the mountain. The magnitudes of the parameters for different experiments are given in Table-I.

Two different groups of initial meteorological data were tested. In the first group we used an analytical initialized data set due to Fritsch *et. al.* (1980). This set of data, horizontally and vertically, have been adjusted and all the observational characteristics of atmosphere such as variation of static stability with height, folding of tropopause, and variation of amplitude and phase of variables with height have been derived and implemented. This group of data is generally made up of sin./cos. functions so they are comparatively easier to deal with and interpret, because the time evolution of their solutions are almost known and the true results are predictable.

The second group of initial data used here, is similar to that used in FW. That is, the velocity vector and temperature distribution vary with height and latitude as follow:

$$t = 0, \qquad \vec{V} = 0, \qquad T = A\tanh(By + y_0) + \Gamma Z \qquad (2)$$

where T (not to confuse with T in table-I) is temperature, A and B indicate the amplitude and gradient of temperature, Γ is the static stability, Z is the height of the grid points, y is the horizontal y components of grid points, and y_0 .is y component of the center of grid. Other variables in this group are set to zero to make the initial condition unbalanced. In the first group the unbalanced condition is made through V, that is, the velocity is set to zero.

(II) *Set-up of the model.* In the model, ground temperature is computed based on the surface energy budget scheme of Blackadar (Zhang and Anthes 1982). Radiation parameterization for shortwave transmissivity is that due to Benjamin (1983). There are five different options for lateral boundary conditions. FW suggested that within the implemented options, the time-dependent inflow-outflow lateral boundary conditions are the most suitable choice. In our experiments, however, lateral boundary values are updated from the initial data every 12 hours. Different grid sizes have been tested based on which two grid sizes of 5 and 10 kilometers have been chosen. Choosing proper magnitude for grid size is vital, because an incorrect value for grid size may result in gross computational errors and inability to resolve the surface topography (Taylor 1980). Different types of lateral boundary conditions were tested, the results of which as well as the results of FW led us to the time-dependent inflow/outflow lateral boundary condition of the model.

4. Discussion of the Results

List of experiments, corresponding parameters, and some results are presented in Table I. There are three groups of data in this table. Experiments C1T1-C1T8, C2T1-C2T3 and C3T1-C3T7. In the first and second groups, the initial data has been designed based on Fritsch initialization method and in the third group is similar to WB temperature distribution and FW initial conditions. The first and second groups are distinguished by a higher temperature gradient in C2T1-C2T3, i.e. in the second group. Here, temperature gradient is controlled by the parameters BY and D2 (refer to Fritsch initialization model). Figures 1 to 4 show the initial and final stable patterns of isotherms in surface level and final configuration of wind along with the vertical cross section of streamlines.

Comparing experiments C1T2, C1T3, C1T5 and C1T6 as regards the time needed for achieving stable conditions (T, in table-I), it can be seen that the magnitude of grid size (Dx) has a small effect on T, such that T is almost independent of Dx. The height of mountain is a crucial parameter influencing T. The higher the mountain, the larger the T, which means that higher mountains prolong the time required for stabilization. Experiments C3T1-C3T4 also support this conclusion. The role of smoothness of the mountain on T is another major factor. The slopes of mountain are defined by a and b, which are equal here because of the bell-shaped mountain used. Results show that steeper mountains delay the adjustment process considerably. Taylor (1981) in his model took into account the slope of mountains with a similar model and found the height and slope of mountain as two determining factors in

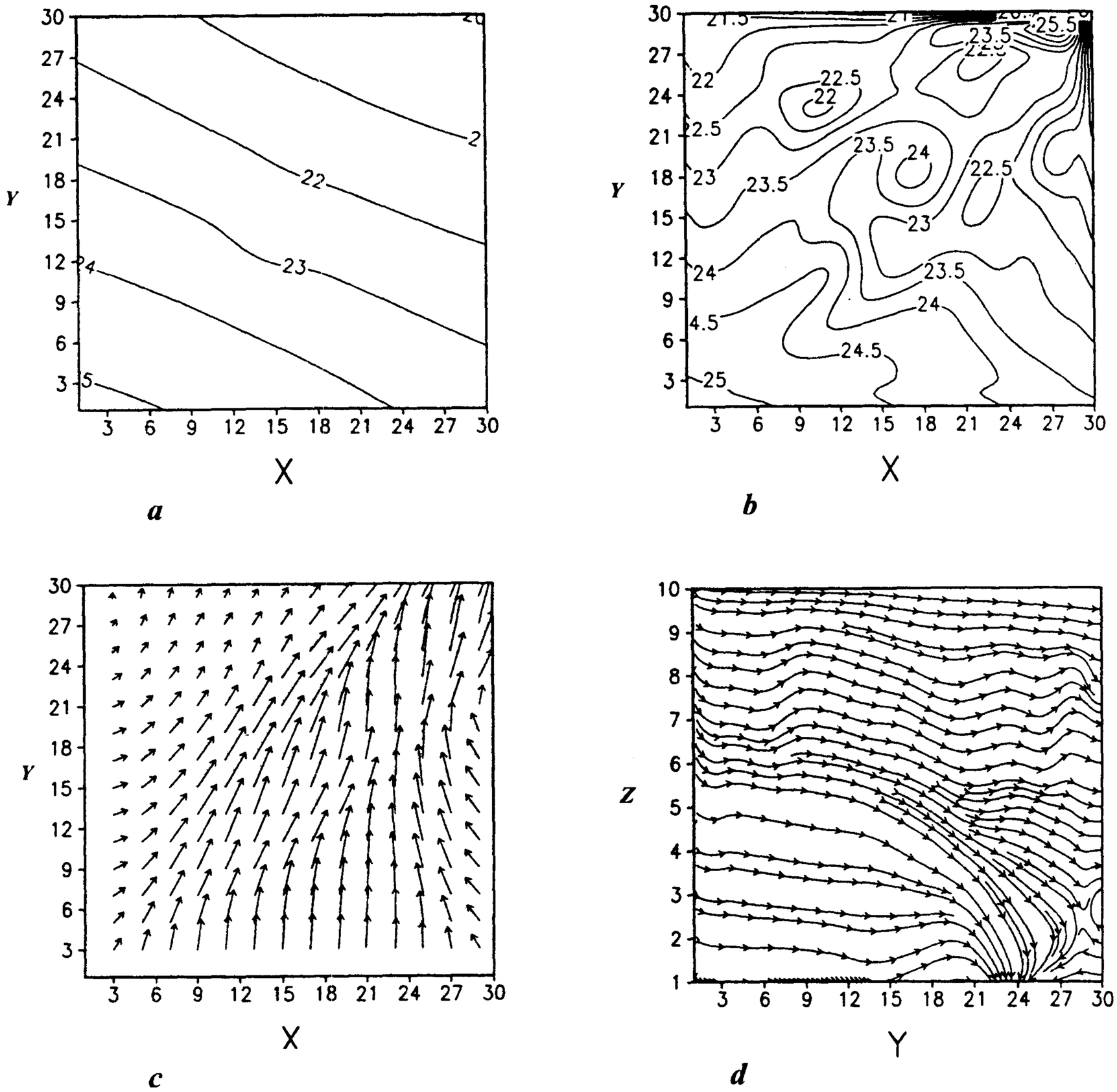

Figure 1. (a) Initial surface temperature distribution for experiment C1T1. In this figure the mountain is located at (15,15) and height of mountain is 500 meters with half width of 10 km, (b) temperature field after adjustment (10 hours of integration), (c) Adjusted wind field at surface, and (d) vertical cross-section of streamlines after achieving stable condition. The vertical coordinate shows the number of σ levels. Z=σ=1 means ground surface, including mountain.

breaking of the flow in lee-side and upstream flow. The breaking of the flow and formation of rotors in lee-side have been seen in our experiments. The higher mountains and larger wind velocities shortened the time of breaking and increased the number of rotors as well.

Regarding the temperature distribution, we found that there is a fall in upstream and a rise in downstream of the mountain. This causes a high-temperature gradient in the mountainous area and it may be thought of as a sort of front formation, however other meteorological variables such as wind and vorticity do not agree with it. The analysis of meteorological data in the vicinity of mountains is difficult. The lower-troposphere temperature patterns predicted by numerical models are contaminated by unacceptable errors. The lower-level temperature for the area near Himalayas, predicted by the Japan Meteorological Agency's numerical model is significantly different from the temperature of the same area. The area that the above high-temperature gradient occurs is mostly in northeast and eastern parts of the mountain, where the blocking of the flow results in an intensified pattern of streamlines in north side of the mountain. In experiment C1T8, in which a front-like pattern of isotherms is seen, the high-

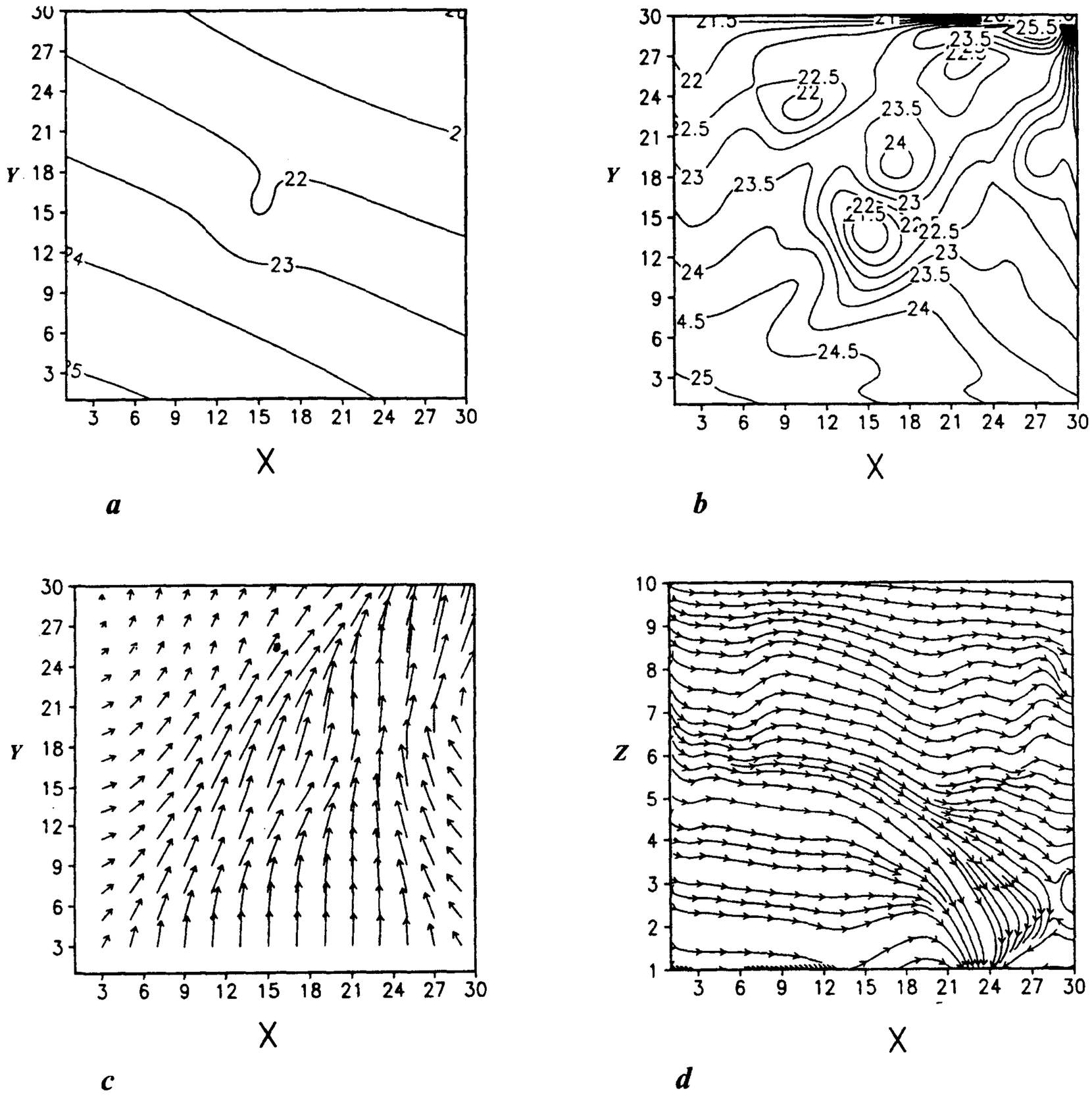

Figure 2. Same as fig.1 but for experiment C1T2 where the height of the mountain is 1000m. The integration time is 11 hours.

temperature gradient is located in lee side with a northwest-southeast axis (Fig 5). This latter event is accompanied by larger magnitudes of vertical velocity and vorticity, as well as considerable changes in wind directions. However its horizontal scale is rather smaller than the typical dimension of fronts.

In their study, WB predicts front formation through the adjustment process. The key assumption in their model seems to be a geostrophic final state. Since in our experiments steady state, equilibrium conditions are not in geostrophic balance, we cannot implement and thus expect the predicted front in WB. Because, existence of roughness in surface level introduces a new force called "drag" or frictional force. In surface and within boundary layer, drag changes the balance of forces in equilibrium state from geostrophic to frictional geostrophic (Salby 1996). The magnitude of vertical velocity, which does not develop in geostrophic balance, has a considerable value by the inclusion of mountain, which in turn does not agree with geostophic configuration of vertical velocity. The frictional effect of mountain is dynamically more frontolysis than frontogenesis. Frictional divergence opposes upward displacement and favors the formation of subsidence inversion, which is well known as a frontolysis process in atmospheric dynamics. At the same time, it reduces the vertical stability. The other fact is that the length of our domain is not consistent with the scales of fronts usually observed on the weather maps.

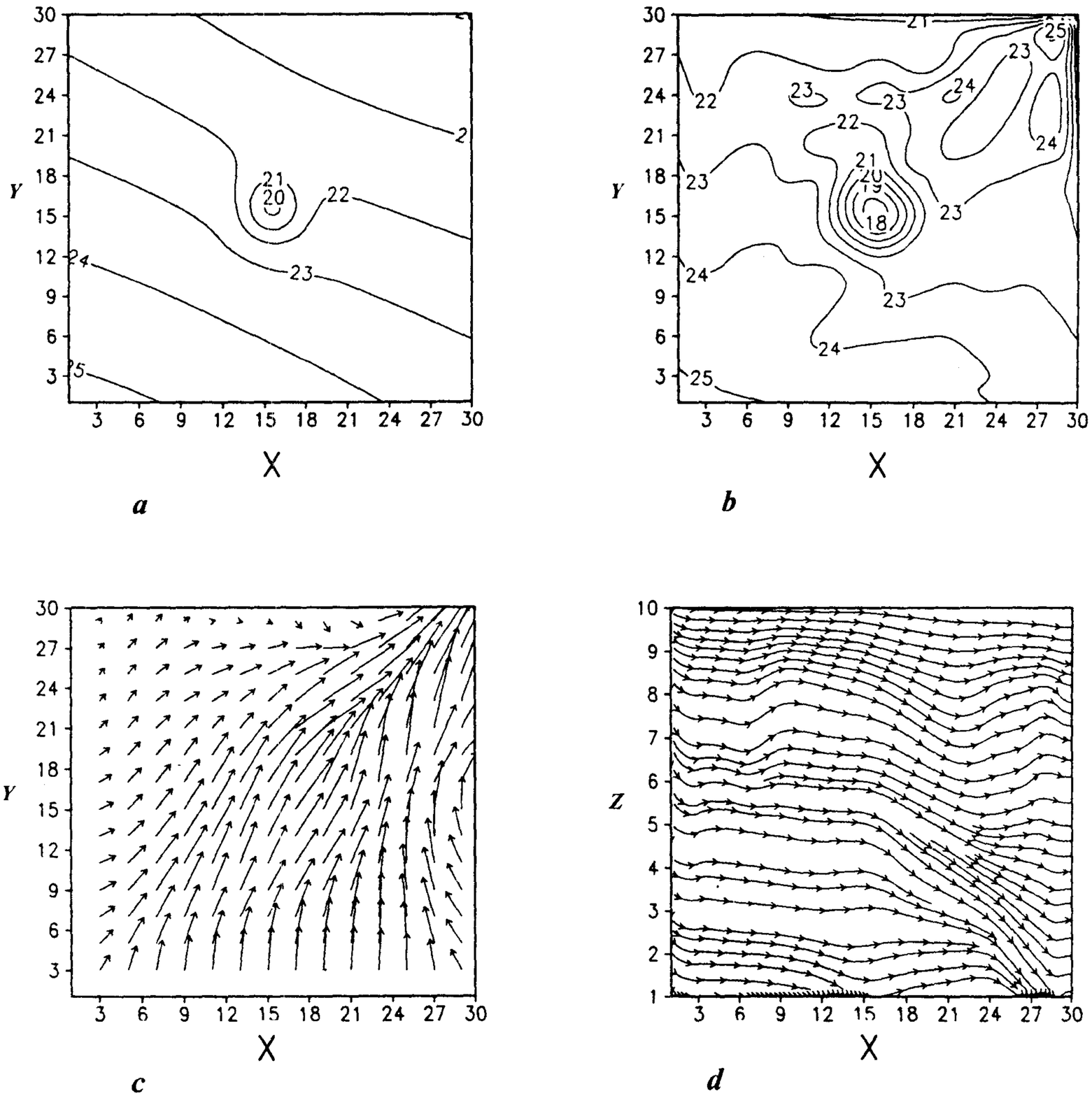

Figure 3. Same as fig.1 but for experiment C1T3 where the height of the mountain is 2000m. The integration time is 15 hours.

5. Energetic of the adjustment

The kinetic energy needed for initially unbalanced atmosphere to reach final, balanced state comes from available potential energy. We note that the initial state is assumed motionless (V=0), and for the final, balanced state V≠0. Therefore, some form of energy has to be transferred to the kinetic energy. Based on WB proposal, this energy is provided by reduction of available potential energy. Also, WB found a proportionality relation between the magnitudes of kinetic energy generated ΔK and the potential energy released ΔP. This ratio $\gamma=\Delta K/\Delta P$ is an indicator of the extent to which geostrophic balance has been achieved. A value of $\gamma=1/2$ was determined by WB for a semigeostrophic model with zero potential vorticity. The magnitudes of γ in our experiments are different from 1/2. If the kinetic energy of geostrophic wind is used for computing γ, the resulting value γ_G is about two orders of magnitude larger than that of WB. If the model predicted actual wind kinetic energy is used for computing γ, the resulting value γ_R is smaller than 1/2 by one order of magnitude. In three experiments (C1T1, C3T1, C3T2) there is a reasonable agreement between resulted values of γ_G and WB's γ. Generally speaking the results of experiments in the third group, are closer to the predicted value by WB than the results of the other two groups. This is because the magnitudes of the meteorological variables in the first and second groups are initially more consistent with stable conditions than in the group 3, and that introducing V=0 in the third group makes the adjustment process more complicated. Introduction of V=0 makes the initially balanced fields unbalanced and triggers a more complicated adjustment

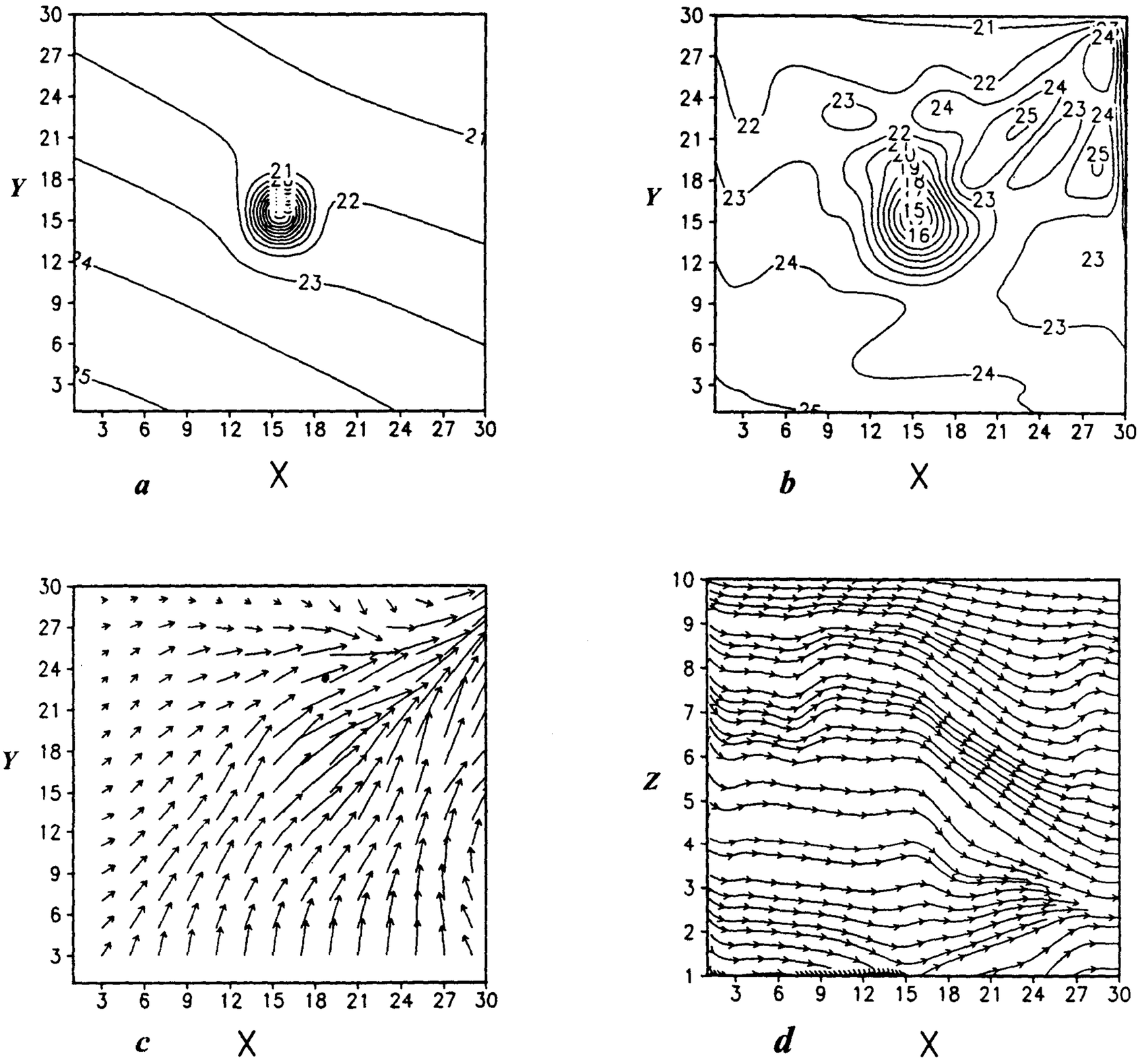

Figure 4. Same as fig.1 but for experiment C1T4 where the height of the mountain is 3000m.

process. In addition, the structure of the initial data in the third group is more similar to the data used by WB than the other two groups, so the resulted values of γ are expected to be closer to WB's value of the γ. From Table-I, we can conclude that there is a direct relation between buoyancy frequency N and γ_R, such that we have smaller γ_R for more stable atmospheric conditions (larger N). Introducing a new force in boundary layer due to the presence of mountains, i. e. drag force, would require a more elaborate analysis of energy, based on which γ needs to be recalculated more accurately.

6. Mountain Drag

In flat-bottom surface layer the only macro-scale force acting on air parcels is shear stress. Including topography in boundary layer results in a new force called drag force.

This force has a considerable role on the balance in the atmosphere and dissipation of energy in boundary layer. Following previous works such as Smith (1978) and Miranda and James(1992), drag is defined as follows:

$$D = \int_0^{L_x} \int_0^{L_y} P_s \nabla h dx dy \qquad (3)$$

where integration is over the entire domain of the model. Table-I shows the magnitude of drag for our experiments after reaching steady-state conditions. There are two sets of normalized drag magnitudes. In the first column, the computed drag over the horizontal

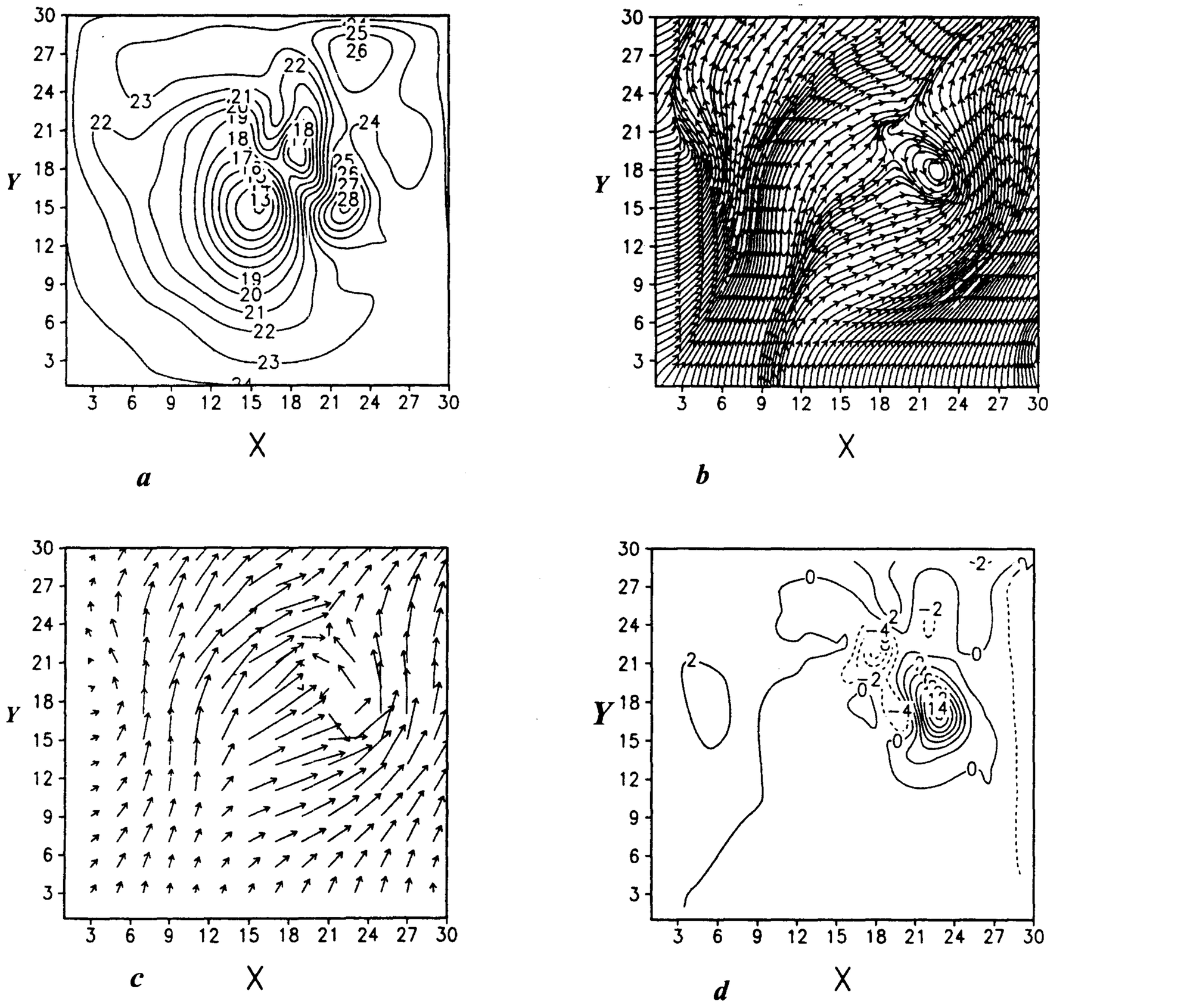

Figure 5. (a) Surface temperature chart after 7 hours of integration for experiment C2T3, (b) streamlines at surface, (c) wind pattern at surface, and (d) vertical vorticity times 10^5 S^{-1}.

domain is normalized by linear hydrostatic magnitude of drag, i.e. $D_{Hydrostatic} = \pi/4\, \rho_0 NUah_0^2$, and in the second column, it has been normalized by linear nonhydrostatic drag (Miranda *et. al.* 1992), $D_{Nonhydrostatic} = \pi/4\, \rho_0 NUah_0^2 \left\{\left[1+\frac{2fa}{U}\right]\exp\left(\frac{-2fa}{U}\right)\right\}$ where U is the wind speed $U = \sqrt{u^2+v^2}$. Smith (1978) suggested 5 possibilities associated with the creation of drag by mountains. Considering different values of the buoyancy frequency N, and the width of mountain, *a*, Smith argues that there is a substantial correlation between these two parameters and drag magnitude (Smith 1978). Consistent with the Smith's argument, table-1 shows that, broader mountains produce higher magnitudes of drag. Separation of flow over mountains, which appears frequently on the maps, is another responsible mechanism for drag formation. As an example of flow separation, figure 6 shows vertical cross section of streamlines of experiment C1T2 after 4 hours of integration. Two rotors at the lee-side of mountain are observed in the figure. Note that since the vertical coordinate in this figure is σ, the separation of flow here means that the separating streamlines originate from the location of the mountain or just behind the mountain. Consequently, we can conclude qualitatively that among

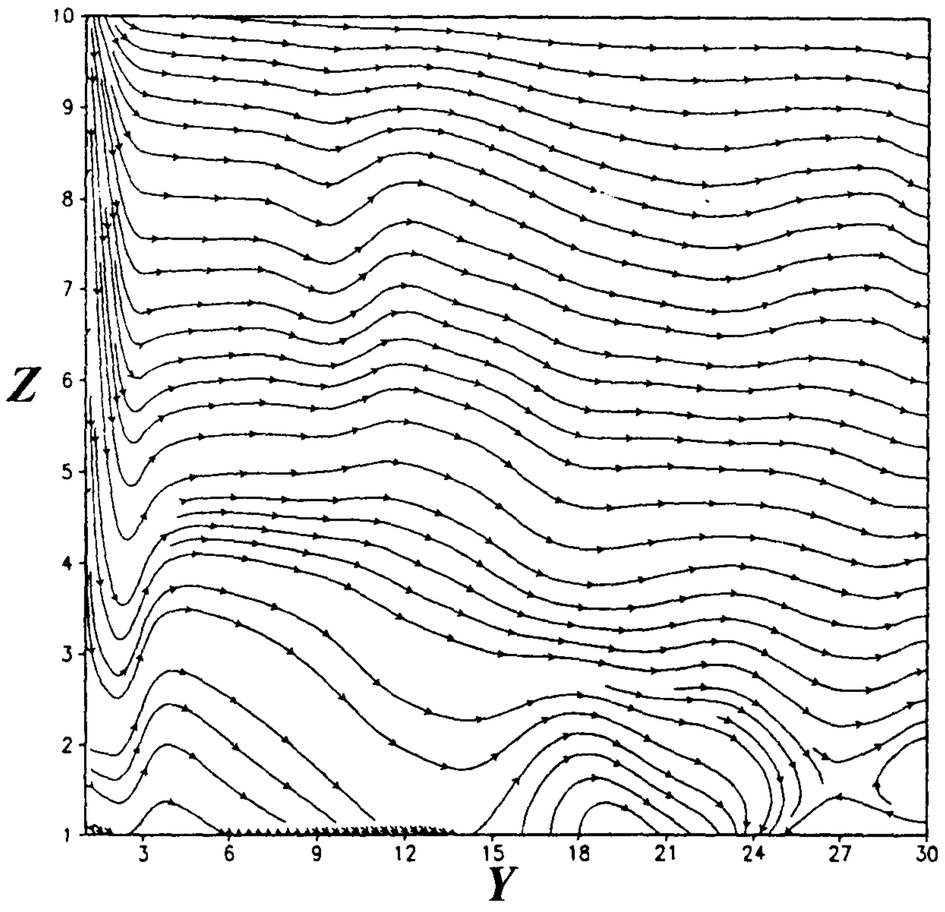

Figure 6. Vertical cross section of streamlines at X=15 for C1T2 after 4hr.

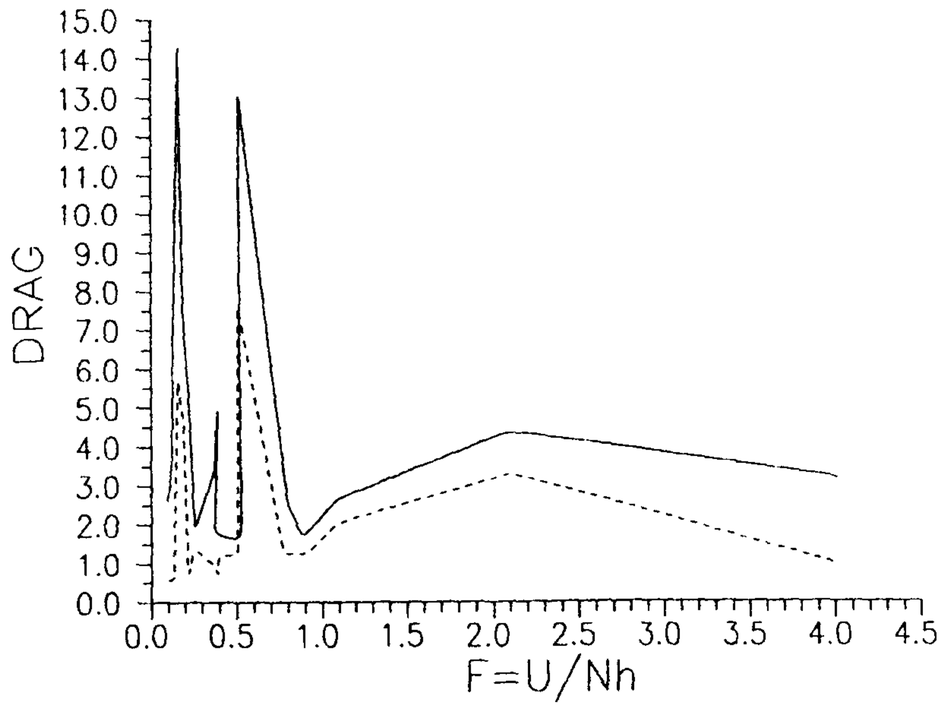

Figure 7. Variation of drag magnitude with Froude number. The solid and dashed lines are the magnitude of drag scaled against its linear hydrostatic ($D_{Hydrostatic}=\pi/4\rho_0 NUah_0^2$)(solid line) and nonhydrostatic (see the text) values (broken line), respectively.

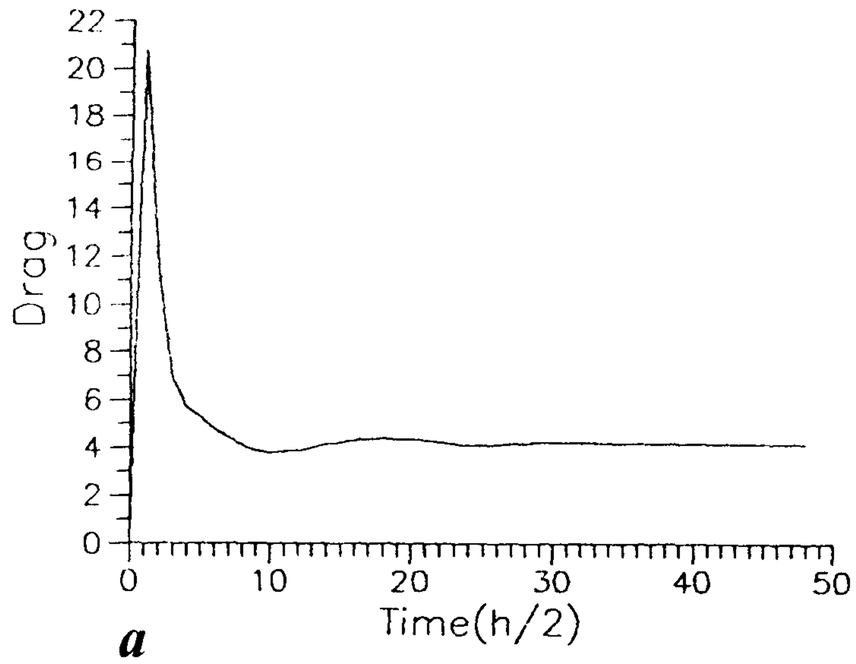

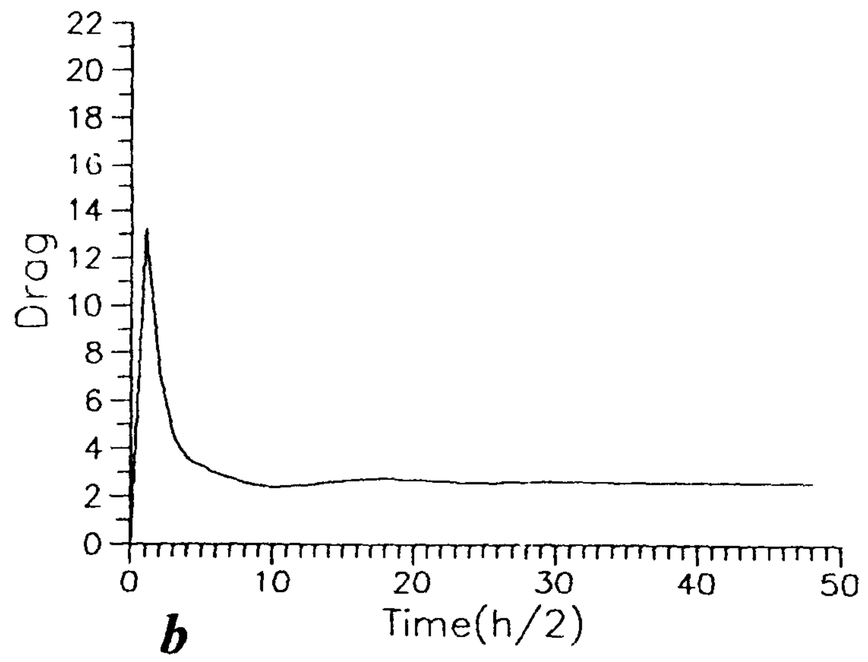

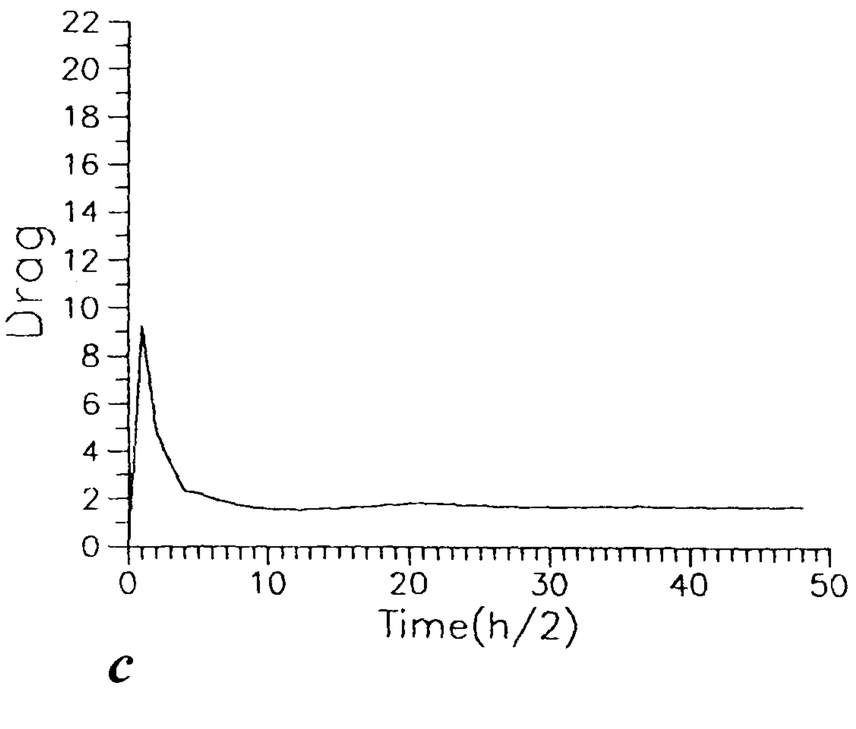

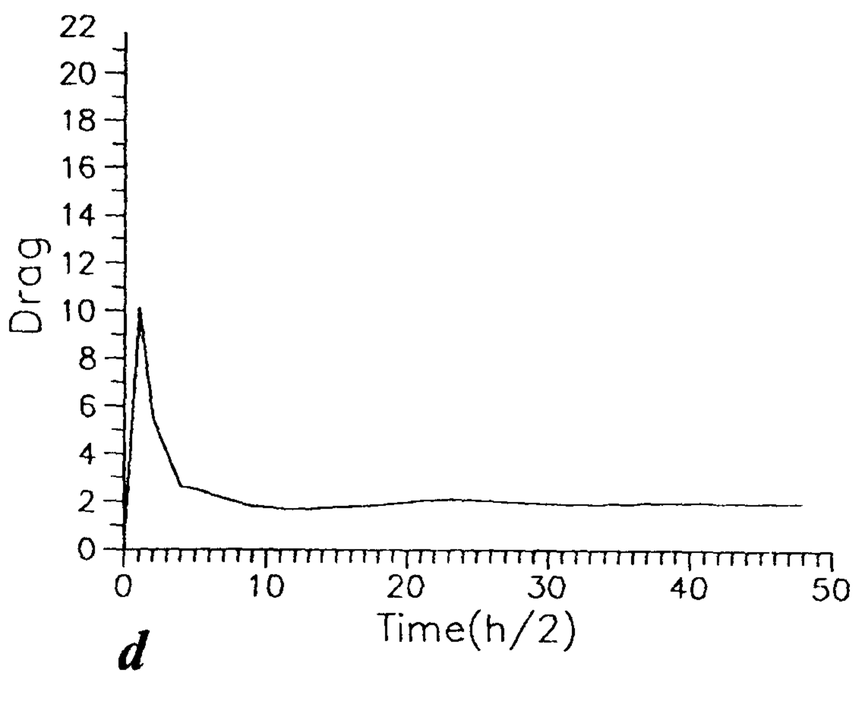

Figure 8. Time variation of drag (normalized by $D_{Hydrostatic}$) for different height of mountains for the experiments (a) C1T1 with h=500m, (b) C1T2 with h=1000m, (c) C1T3 with h=2000m, and (d) C1T4 with h=3000m.

5 possibilities mentioned by Smith, flow separation and drag due to vertically propagating internal gravity waves seem to be more responsible for drag.

Relation between Froude number (U/Nh_0) and value of drag is another important sign of presence of mountain barrier in boundary layer. Figure 7 indicates the variation with Froude number of drag magnitude divided by the corresponding theoretical values for drag in linear hydrostatic and nonhydrostatic models. As it is clear there are 3 regimes of variation of values of Froude number (F) presented in this column. These 3 different regimes of variation of D with F are those corresponding to $0< F<1$, $1<F<2$ and $F>2$. In the first region, i.e. for $0<F<1$, there is an intense oscillation of drag. Miranda and James found that in region $F<0.5$ there is a continuous increase in drag values, but here what we observe is an almost equal in magnitude decrease in D in addition to the increase. In region $0.5<F<1$, they showed a reduction of D with increasing F. Here we see that a rise of D followed by a drop. In the second domain, $1<F<2$, we see a smooth growth of D with F, opposite to Miranda and James smooth fall of D. For $F>2$, the results agree with linear gravity-wave theory of Smith (1980).

Finally, to see the variation of drag with time as well as the height of mountain, four graphs are presented. Figs. 8-a to 8-d, present the change of D with time for different heights of mountains, Fig. 8-a for 500m, 8-b for 1000m, 8-c for 2000m, and 8-d for 3000 meter heights. Their common feature is that almost in less than 5 hours the drag reaches its stable value. In first 5 hours, we see an oscillation in D, the amplitude of which is higher for flatter mountains.

7. Conclusions

The final, stable, steady-state of the atmosphere in the presence of topography is frictional geostrophic, not purely geostrophic condition. This effect changes the regime of flow in the free atmosphere and excites the gravity waves. Breaking of the flow at the lee-side of the mountain is observed. Higher and steeper mountain enhances the breaking of the flow in the lee-side.

Front formation, which happens in geostrophic adjustment process in some especial cases, was not observed here. In one case, although a high-temperature gradient in surface is formed and the other meteorological variables and parameters agree with a frontal feature, its horizontal scale is smaller than that of a classic front.

Time needed for achieving stable condition by the atmosphere has a direct relation with the height of the mountain. Higher mountains prolong the time of the adjustment process. The higher a mountain is, the longer is the time it takes for the atmosphere to achieve steady-state condition. The slope of mountain influences the stabilization time T significantly. Mountains with larger slopes delay the adjustment considerably.

Magnitude of grid size has less influence on the period of adjustment process, but it has a considerable effect on the drag magnitude of the mountain. Since smaller grid sizes can resolve the roughness of the surface more accurately, it seems that with decreasing grid size the drag magnitude increases.

Values of the potential energy released and the kinetic energy produced do not agree with the corresponding magnitudes as predicted by previous works on geostrophic adjustment process in the absence of topography. On the one hand, the kinetic energy of the geostrophic wind is larger than that predicted by the theory of geostrophic adjustment, and on the other hand the kinetic energy of the actual, model wind is smaller than that predicted by the theory of geostrophic adjustment. Also there is a reasonable link between the buoyancy frequency and geostrophic kinetic energy. The more stable the condition, the smaller the value of kinetic energy.

Among five possibilities suggested by Smith about mountain drag, two of them are dominant. These two mechanisms are flow separation in lee side and vertically propagating internal gravity waves. Regarding the relation of drag and Froude number, for small Froude number ($F<1$) there are some inconsistencies with other studies. The time needed for drag to reach its stable magnitude does not vary with height of the mountain very much.

Acknowledgements

We thank Dr. Wang Yuan and Dr. Alireza Mohebalhojeh for their careful reading and making helpful suggestions. Also great thanks go to the staffs, colleagues and students working in the Laboratory of Mesoscale Severe Weather of Nanjing University. The first author would like to express his appreciation to the members of the department of Meteorology of the University of Reading for their kind cooperation and permission to use documents of their library.
The second author would like to express his thanks to the China's government for supporting this work under "Severe meso-scale meteorology" grant and NSF projects: 49735180, 49675259.

References

Anthes, R. A. and Warner, T. T., 1978, Development of hydrodynamic models suitable for air pollution and

other mesometeorological studies. *Mon. Wea. Rev.* **106**, 1045-1078.

Benjamins, S. G., 1983, Some effects of surface heating and topography on the regional severe storm environment. Ph.D. thesis, Department of Meteorology, The Pennsylvania State University, 265 pp.

Blumen, W. and Wu, R., 1995, Geostrophic adjustment, frontogenesis and energy conversion; *J. Phys. Oceanogr.*, **25**, 428-438.

Eliassen, A. and Palm, E., 1961, On the transfer of energy in stationary mountain waves. *Geofys. publ. Oslo*, **22(3)**, 1-23.

Farahani, M. M., and Wu, R., 1998, A numerical study of Geostrophic adjustment and frontogenesis. *Advances In Atmospheric Sciences,* **15**, 179-192.

Fritsch, J. M., Magaziner, E. L. and Chappel, C. F., 1980, Analytical initialization for three-dimensional numerical models. *J. Appl. Meteor.*, **19**, 809-818.

Haltiner, G. J. and Williams, R. T., 1980, Numerical prediction and dynamic meteorology. John Wiley & Sons, 477 pp.

Hsie, E. Y., 1987, MM4 (Penn state/NCAR) Meso-scale model version 4 documentation. *NCAR Tech. Note, NCAR/TN-294+STR,* 215 pp.

Keyser, D. and Shapiro, A., 1986, A review of the structure and dynamics of upper-level frontal zones. *Mon. Wea. Rev.*, **114**, 452-494.

Mc Farlane, N. A., 1987, The effect of orographically excited gravity wave drag in the general circulation of the lower stratosphere and troposphere. *J. Atmos. Sci.*, **44**, 1775-1800.

Miranda, P. M. A., and James, I. N., 1992, Non-linear three dimensional effects on gravity-wave drag: Splitting flow and breaking waves. *Q. J. Royal Meteorol. Soc.*, **118**, 1057-1081.

Ou, H. W., 1984, Geostrophic adjustment: A Mechanism for frontogenesis. *J. Phys. Oceanogr.*, **14**, 994-1000.

Palmer, T. N., Schutts, G. J. and Swinbank, R., 1986, Alleviation of a systematic westerly bias in general circulation and numerical weather prediction models through an orographic gravity wave drag parametrization. *Q. J. Royal Meteorol. Soc.*, **112**, 1001-1039.

Salby, M. L., 1996, Atmospheric Physics. Academic Press Limited, London, 627 pp.

Smith, R. B., 1978, A measurment of mountain drag. *J. Atmos. Sci.*, **35**, 1644-1654.

Smith, R. B., 1980, Linear theory of stratified hydrostatic flow past an isolated mountain. *Tellus,* **32**, 348-364.

Taylor, P. A., 1981, Model predictions of neutrally stratified planetary boundary over ridges. *Q. J. Royal Meteorol. Soc.*, **107**, 111-120.

Taylor, P. A. and Cent, P. R., 1980, Modification of the Boundary Layer by Orography. In " Orographic effects in planetary flows" *GARP publ. ser. No. 23, WMO- ICSU, Geneva* , pp 143-166.

Wu, R. and Blumen, W., 1995, Geostrophic adjustment of a zero potential vorticity flow initiated by a mass imbalance. *J. Phys. Oceanogr.*, **25**, 439-445.

Zhang, D. L. and Anthes, R. A., 1982, A high-resolution model of the planetary boundary layer-sensitivity tests and Comparisons with SESAME-79 data. *J. Appl. Meteor.*, **21**, 1594-1609.